Journal of Catalysis **187,** 474–485 (1999)
Article ID jcat.1999.2624, available online at http://www.idealibrary.com on IDEAL®

# Influence of Ceria on Pd Activity for the $CO + O_2$ Reaction

M. Fernández-García,*,[1] A. Martínez-Arias,* L. N. Salamanca,* J. M. Coronado,*,† J. A. Anderson,† J. C. Conesa,* and J. Soria*

*Instituto de Catálisis y Petroleoquímica, CSIC, Campus Cantoblanco, 28049-Madrid, Spain; and †Dept. of Chemistry, University of Dundee, Dundee DD1 4HN, Scotland,United Kingdom

Received April 19, 1999; revised June 24, 1999; accepted June 24, 1999

**The behavior of a series of palladium catalysts supported on alumina, ceria, and ceria/alumina for the $CO + O_2$ reaction has been analyzed by a combination of electron transmission microscopy, infrared and electron paramagnetic resonance spectroscopies, and catalytic test studies. Ceria is shown to decrease the onset of the reaction by ca. 130 K due to an enhanced activation of both reactant molecules. Even at room temperature, ceria facilitates activation of CO by promoting the formation of metallic palladium and that of oxygen by the presence of reactive vacancies at the Pd–Ce interface. The optimum ceria promoting effect in the CO conversion is observed for palladium particles in contact with 3-dimensional ceria supported particles, which seem to be oriented by their interaction with alumina, and ascribed to the specific characteristics of the anionic vacancies located at the corresponding Pd–Ce interface. The bulk ceria support, however, induces an oxidation–deactivation process of palladium at medium and high reaction temperatures which hinders reaction between Pd-bonded CO and Ce-bonded oxygen at the Pd–Ce interface.** 

## I. INTRODUCTION

Cerium oxide is a commonly used promoter in current automobile catalysts used in the control of pollutant gas emissions (CO, NO, and hydrocarbons). Ceria is thought to play a number of roles in these catalysts. The Ce(IV)/Ce(III) redox pair may store/release gases under oxidizing/reduction conditions, extending the operational window centered close to stoichiometry (1–3). Ceria also increases the thermal stability of the alumina support, yielding more durable catalysts (4). Additionally, metal–ceria interactions lead to several beneficial effects, including increasing the dispersion of the active components (5, 6) and promoting the activation of molecules such as CO or NO (7). The large dispersions observed are usually explained by the important interactions between the active metal cations and ceria produced during the preparation stage. The ease with which oxygen vacancies of the ceria component are formed and/or reoxidized is believed to influence the extent of the source/sink of active oxygen that results in the oxidation/reduction of pollutant molecules (8). Current research involving three-way catalysts (TWCs) is mainly directed toward the elucidation of details relating to the role of the metal–reducible oxide mutual influence on the activation of reactants and the consequences for the overall activity.

Pd is a promising addition to current TWC formulations and behaves particularly well when compared with Pt and Rh-based catalysts for low-temperature oxidation of CO and hydrocarbons (9). The specific chemical basis for this behavior is still not clear. Recent studies involving Cu- (10–12) and Pt- (13, 14) based catalysts indicate that metal–ceria interactions involve electronic contact between the components that allow synergetic oxidation/reduction of both the active metal and the ceria support, favoring the catalytic performance of these systems over a wide range of experimental conditions. In an attempt to analyze this situation for Pd–Ce catalysts, the activity of a series of Pd-supported catalysts has been tested in the $CO + O_2$ reaction. The series contains ceria, alumina, and ceria/alumina as supports. Catalysts were characterized using transmission electron microscopy (TEM) and their behavior under reaction conditions followed using infrared spectroscopy (DRIFTS). The existence of oxygen vacancies for the oxide components and the influence of these on the reaction have been studied by electron paramagnetic resonance (EPR) using as a probe the superoxide ($O_2^-$) radical detected after oxygen adsorption.

## II. EXPERIMENTAL

Two $CeO_x/Al_2O_3$ supports were prepared by incipient wetness impregnation of an alumina powder (Condea Puralox, $S_{BET} = 180\ m^2\,g^{-1}$) with an aqueous solution of $Ce(NO_3)_4 \cdot 6H_2O$, corresponding to a 10 and 39 wt% content of $CeO_2$. After drying at 353 K, the supports were calcined at 773 K for 6 h under dry air. These supports, 10CA and 39CA, the parent alumina, A, and a cerium oxide (C, Rhône-Poulenc, $S_{BET} = 287\ m^2\,g^{-1}$) were impregnated with aqueous $Pd(NO_3)_2 \cdot xH_2O$ to give a 0.5 wt% metal

[1] To whom correspondence should be addressed. E-mail: icpmf03@pinar1.csic.es; Fax: 34-91-5854760.



0021-9517/99 $30.00

loading. Catalysts were calcined following the above drying/calcination procedure.

Catalytic tests using a 1% CO + 0.5% $O_2$ ($N_2$ balance) at 30.000 $h^{-1}$ were performed in a glass reactor system. Gases were controlled with mass flow controllers and analyzed on line using a Perkin-Elmer 1725X FTIR spectrometer coupled with a multiple reflection transmission cell (Infrared Analysis, Inc.). Oxygen concentrations were determined using a paramagnetic analyzer (Servomex 540A). Prior to catalytic testing, an *in situ* calcination in dry air at 773 K was performed, followed by cooling in the same atmosphere and purging in $N_2$ at room temperature (RT). A characteristic test consisted of increasing the temperature from 298 to 823 K at 5 $K \cdot min^{-1}$.

TEM experiments were carried out using a JEOL 2000 FX (0.31 nm point resolution) equipped with a LINK (AN 10000) probe for EDS analysis. Portions of samples were crushed in an agate morter and suspended in cyclohexene. After ultrasonic dispersion, a droplet was deposited on a copper grid supporting a perforated carbon film. Micrographs and electron diffractograms were recorded over selected areas with compositions previously characterized by EDS.

DRIFTS analysis of adsorbed species present on the catalyst surface under reaction conditions was performed using a Perkin–Elmer 1750 FTIR fitted with an MCT detector. The DRIFTS cell (Harrick) was fitted with $CaF_2$ windows and a heating cartridge that allowed samples to be heated to 773 K. Samples of ca. 80 mg were calcined *in situ* (as before) and then cooled to 298 K before introducing the reaction mixture and heating at 5 $K \cdot min^{-1}$ to 673 K, recording one spectrum (4 $cm^{-1}$ resolution) every 15 K. The gas mixture (1% CO, 0.5% $O_2$, $N_2$ balance) was prepared using a computer controlled gas-blender with 75 $cm^3 \cdot min^{-1}$ passing through the catalyst bed.

EPR spectra were recorded at 77 K with a Bruker ER 200 D spectrometer operating in the X-band and calibrated with a DPPH standard ($g = 2.0036$). Portions of ca. 40 mg were placed inside a quartz probe cell with greaseless stopcocks. A conventional high-vacuum line was used for different treatments. *In situ* precalcined samples (as before) were reduced with 100 Torr of CO at increasing temperatures (298, 373, and 473 K) for 1 h and evacuated for 30 min at the same temperature. Alternatively, samples were treated with a stoichiometric mixture of $CO + O_2$ (700 $\mu$mol of CO and 350 $\mu$mol of $O_2$ per gram of sample) at 323, 423, and 523 K. Over these preconditioned surfaces, oxygen adsorption was performed at 77 K, using doses of 70 $\mu mol \cdot g^{-1}$ except otherwise specified, followed by outgassing at the same temperature (residual pressure $2 \times 10^{-4}$ mbar) and oxygen-related radicals detected by EPR (without intermediate warming to RT). Some oxygen adsorption experiments continued (when specified) by warming the sample to RT during 30 min and recording new spectra at 77 K.

## III. RESULTS

### *$CO + O_2$ Catalytic Activity*

Results of light-off tests for the four Pd catalysts are presented in Fig. 1. Initial contact of Ce-containing samples with the reaction mixture caused a 10–20 K temperature increase that fell to RT after a few minutes except in the case of Pd39CA, where a temperature of ca. 333 K was maintained with full CO conversion. As with typical noble TWC formulations, Pd/CA catalysts show enhanced activity when compared with Pd on the individual oxides. The percentage of ceria loaded in the mixed CA support does not significantly affect the catalytic performance of the Pd systems, although a larger conversion is observed for Pd39CA at low temperature. The PdC catalyst shows a distinct, unique behavior: at low temperature it shows activity similar to that of Pd10CA but around 373 K it reaches a plateau in which CO conversion remains nearly constant till ca. 473 K and then finally displays a gradual increase in conversion to 100% at 550 K. Cooling of PdC in the reaction mixture produced a similar conversion/temperature curve and a 2nd light-off run, using the same catalyst sample, exhibited similar (slightly improved) light-off behavior but with a less pronounced plateau (dashed line in Fig. 1).

With the exception of ceria alone, the supports show negligible contributions to catalytic conversion (not shown). Light-off tests show significant activity of the neat ceria material above 523 K giving 30 and 70% CO conversion at 550 and 600 K, respectively.

### *TEM*

The EDS/diffraction study of the samples (Table 1, Fig. 2) did not detect Pd except in a small concentration in the Ce-rich zones of the Pd39CA sample. The ceria component

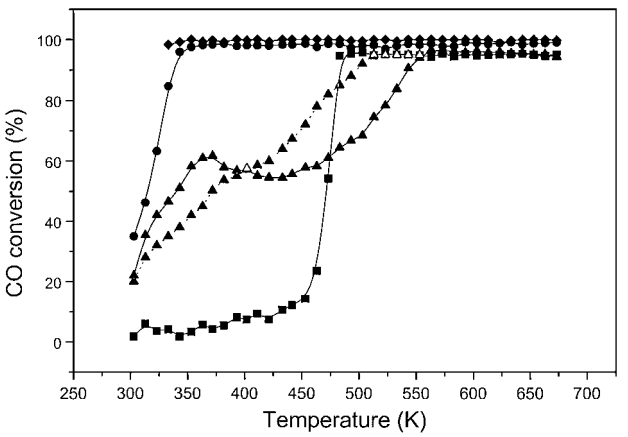


**FIG. 1.** CO conversion profiles for the $CO + O_2$ reaction in Palladium samples: Solid line, first run; dashed line, second run. Triangles, PdC; rhombs, Pd39CA; circles, Pd10CA; squares, PdA. See text for details.

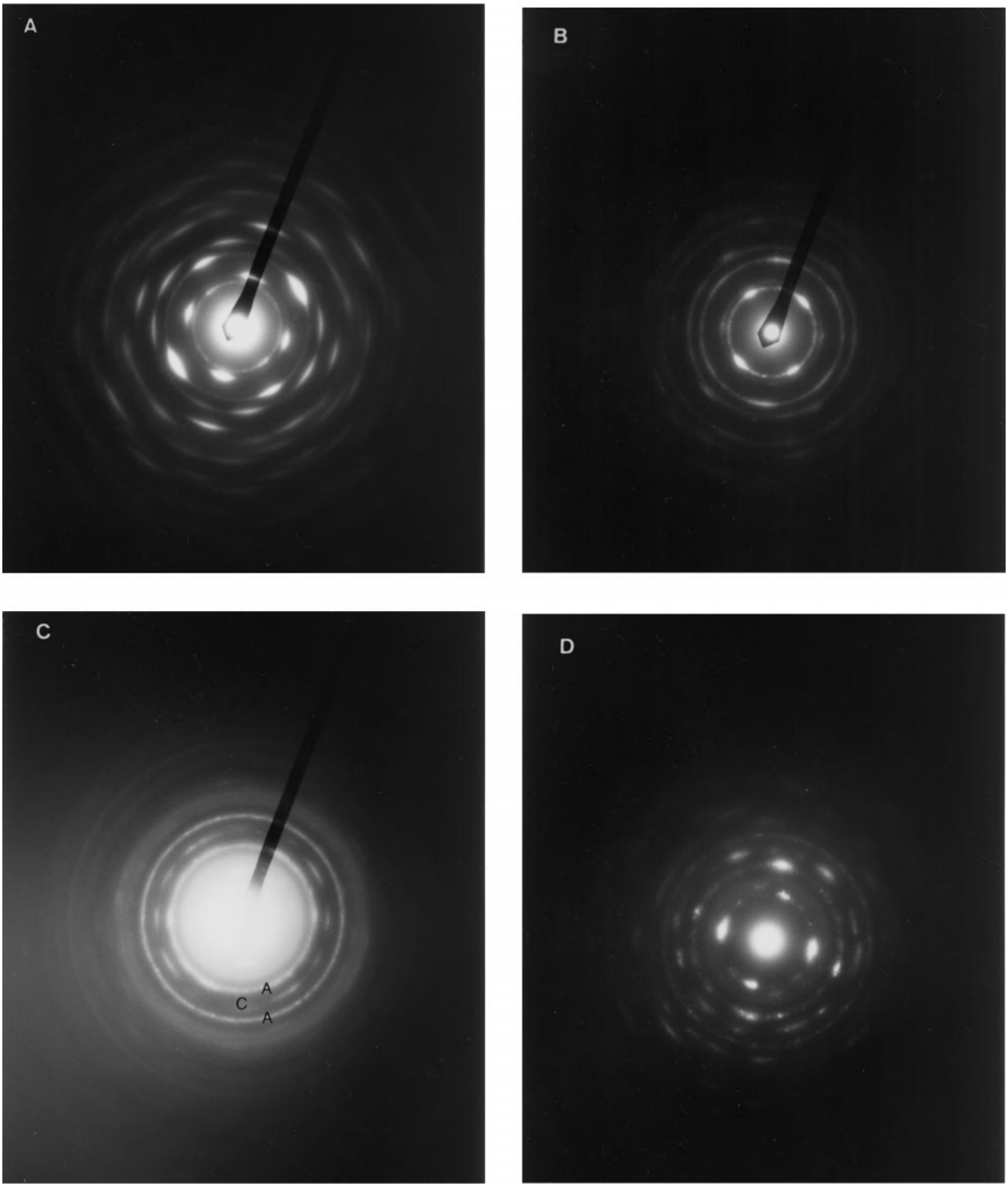


**FIG. 2.** Electron diffraction diagrams for different zones of Pd specimens. (A, B) PdC; (C, D) Pd39CA; (E, F) Pd10CA. C, E rings are assigned to: (A) alumina and (C) ceria components. In (A) a diffraction pattern of a [001]-oriented $CeO_2$ crystal is presented. In (B, D, and F) diffraction patterns of [011]-oriented $CeO_2$ crystals are presented.

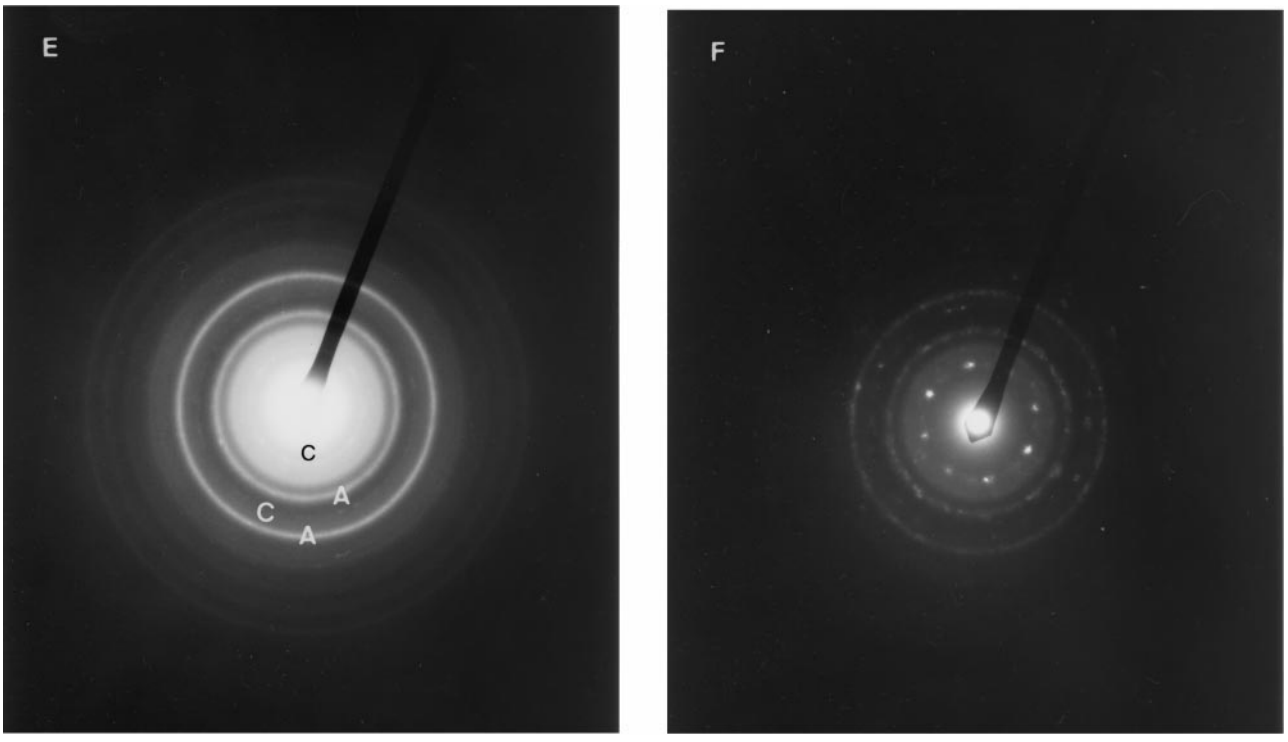


**FIG. 2**—*Continued*

appeared to be (reasonably) homogeneously dispersed in the Pd10CA catalyst while the Pd39CA catalyst clearly contained Ce-rich and Al-rich zones (Table 1). Dark-field images taken from the first two diffraction lines of ceria (i.e., (111) and (200)) allow estimation of an average particle diameter of 6 nm for the diffracting ceria particles in contact with alumina of the Pd10CA sample and 11 nm for those in the Ce-poor zones of Pd39CA. For the Ce-rich zones of the latter sample, the ceria entities are considerably larger containing contributions from particles with diameters up to ca. 150 nm. The PdC sample shows an average particle size of 2.7 nm.

The electron diffractograms show that the $CeO_2$ diffracting domains in the particle aggregates present in sample PdC and C material are strongly oriented on the supporting TEM grid, so that the patterns show consistently orientations with zone axes [001] and [011] parallel to the electron beam (Figs. 2a and 2b). Microscopy analysis of both samples was performed in great detail for several ceria particles and spot sets corresponding to other zone axes, e.g. [111], were not detected. In contrast, ceria in the mixed support samples do not show such a characteristic marked orientation: almost continuous more or less spotty rings appear in many regions of the samples (Figs. 2c–2f). However, in some areas it is possible to identify majority contributions of a set of spots which indicate the dominant presence of particles mainly oriented along one zone axis. Whenever such a thing happens, the identified zone axis corresponds to the [011] direction (Figs. 2d and 2f). Concomitantly to ceria, the alumina rings also appear spotty in these sample areas. This is observed equally in Pd10CA and Pd39CA and indicates the presence of specific preferential orientations of ceria crystallites in the mixed support samples.

**TABLE 1**

**Ce/Al and Pd/Al Atomic Ratios Obtained with EDS**

| Sample | Ce/Al | Pd/Al |
|---|---|---|
| PdA | — | n.d. |
| Pd10CA | 0.03–0.10 | n.d. |
| Pd39CA | 0.04–1.04 | 0.00–0.04 |
| PdC | — | n.d.[a] |

*Note.* n.d., Pd not detectable.
[a] Pd/Ce ratio.

### *IR Experiments*

Exposure of the calcined samples to 15 Torr of CO at RT gave rise to bands in the 1800–2250 $cm^{-1}$ interval (Fig. 3). Apart from the CO gas contributions at 2175/2125 $cm^{-1}$ and a negative band originated by an incomplete subtraction with the background spectrum of the $CO_2$ gas contribution,

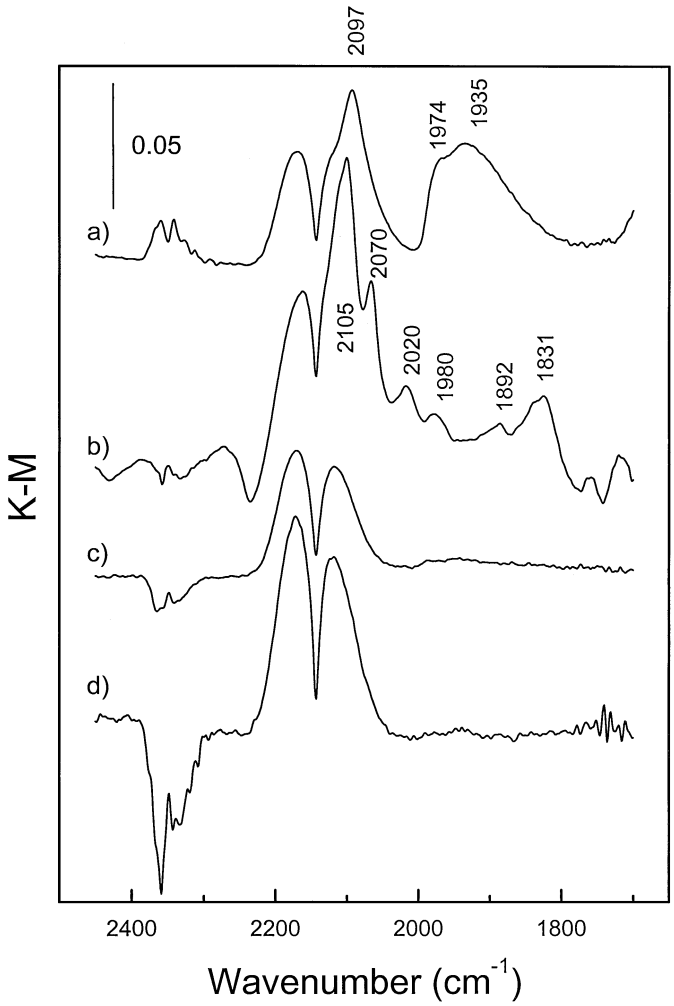


**FIG. 3.** IR spectra after CO adsorption at RT on calcined samples. (A) PdC; (B) Pd39CA; (C) Pd10CA; and (D) PdA.

PdC (Fig. 3a) and Pd39CA (Fig. 3b) show mainly contributions below 2100 $cm^{-1}$ due to CO adsorption at reduced Pd sites (14–16), while the remaining catalysts (Figs. 3c and 3d) show only rather weak maxima located above 2150 $cm^{-1}$ (Pd10CA and PdA), the latter being visible only after flushing of CO gas from the chamber. The ceria-supported sample gives well defined, relatively large $Pd^0$ particles while the mixed oxide supports contained a more heterogeneous variety of Pd entities as indicated by the number of IR bands detected.

DRIFT spectra recorded under reaction conditions with increasing temperature (Figs. 4A–4C) indicate a progressive decrease in CO gas contribution (2175/2125 $cm^{-1}$) and an increase in $CO_2$ (ca. 2350 $cm^{-1}$) providing an approximate correlation with light-off plots (Fig. 1). For the CA-supported sample, an almost complete elimination of the gaseous CO with a large increase in $CO_2$ is achieved whereas the decrease in CO gas is much less for PdC and a plateau in the production of $CO_2$ is established for $T > 400$ K. In the case of PdC, the $CO_2$ yield does not increase to the extent predicted from the light-off plots at temperatures beyond the plateau region. This may indicate that the relatively slow oxidation occurring over the support does not allow equilibrium to be established using the relatively high space velocities passing through the IR cell. All catalysts present an asymmetric shaped band around 1980–1970 $cm^{-1}$, corresponding to islands of adsorbed CO molecules each bridging two $Pd^0$ atoms (15). These islands appear after contact with the reaction mixture from 298 K for ceria containing samples, while for the alumina supported sample, they were observed as a weak feature at 323 K, which grew in intensity and underwent a progressive, continual displacement from 1978 $cm^{-1}$ at 373 K to 1967 $cm^{-1}$ at 473 K. In contrast, the intensity and frequency of this band remain constant for Pd10CA until 400 K, where it was displaced to 1960 $cm^{-1}$ before disappearing above 473 K. For PdC, the invariance at 1975 $cm^{-1}$ was maintained until ca. 420 K, before being shifted to lower frequencies but never being eliminated from the spectrum, even with the sample at 598 K (Fig. 4A(k)). An additional weak band at 2089 $cm^{-1}$ for PdC, superimposed on the CO gas phase band contribution and due to linearly adsorbed CO at $Pd^0$ sites (15), was observed over the range 298 to 400 K. This carbonyl species was also observed for PdA, first superimposed on the CO gas phase contribution and centered at 2099 $cm^{-1}$ at 373 K (Fig. 4C(c)) and undergoing a continual red shift to give a band at 1967 $cm^{-1}$ at 473 K (Fig. 4C(h)). In the 420–500 K temperature range, the spectra of the PdC catalyst shows additional features at 2192 and 2152 $cm^{-1}$. The first can be assigned to CO adsorption on $Pd^{2+}$ sites while the second may be assigned to carbonyls adsorbed on $Pd^{2+}$ or $Ce^{3+}$ entities (14, 15, 17). These two peaks were never detected in experiments carried out for Pd39CA (not shown) or Pd10CA. An interaction between $CO_2$ and the support is responsible for the band at ca. 2310 $cm^{-1}$ for PdC.

### *EPR Experiments*

Weak features at $g = 2.16$, 2.06, 2.03, and 2.01 are observed in the EPR spectra of PdA reduced in CO at 298 or 373 K, indicating the presence of small amounts of $Pd^+$ or $Pd^+$-carbonyl species produced by those treatments (18). No EPR signal was detected after reduction treatment at 473 or 573 K. No new signals appear after oxygen adsorption at 77 or 298 K on CO prereduced samples.

For cerium-containing samples, a weak, narrow signal at $g_\perp = 1.967$ and $g_\parallel = 1.947$–1.941 was observed after calcination. This has been attributed to $Ce^{3+}$ ions or electrons trapped at oxygen vacancies in the neighborhood of $Ce^{3+}$, these defects being stabilized by closely located impurities (19). Other minor signals for Pd10CA and Pd39CA appear as a hyperfine multiplet of six symmetric lines centered at

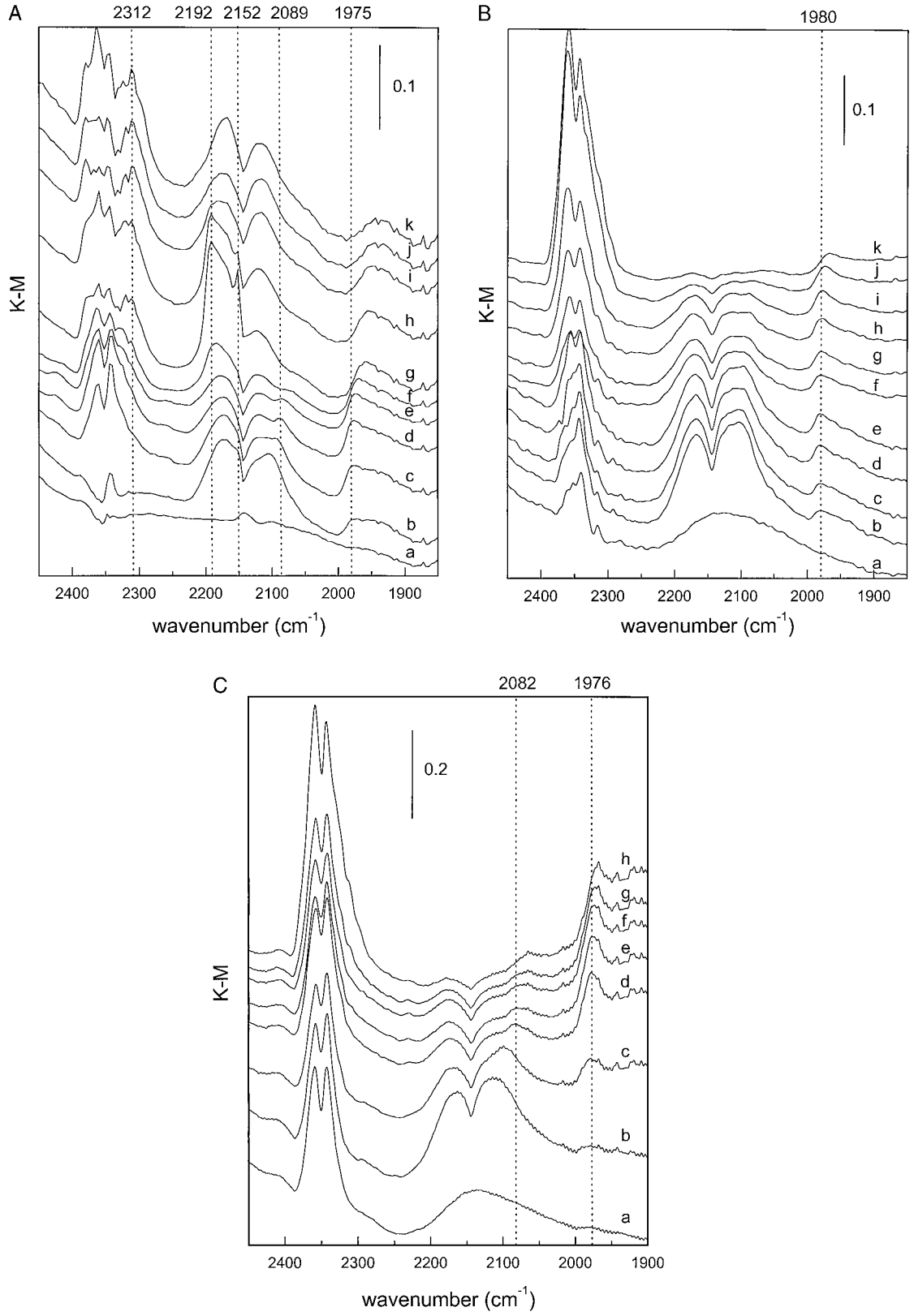


**FIG. 4.** (A) IR spectra of PdC sample in a flow of (a) 0.5% of $O_2$ in nitrogen at 297 K, then 1% CO, 0.5% $O_2$, $N_2$ balance at (b) 297; (c) 343; (d) 358; (e) 373; (f) 388; (g) 418; (h) 478; (i) 508; (j) 569; and (k) 598 K. (B) IR spectra of Pd10CA sample in a flow of (a) 0.5% of $O_2$ in nitrogen at 289 K, then 1% CO, 0.5% $O_2$, $N_2$ balance at (b) 289; (c) 299; (d) 308; (e) 321; (f) 333; (g) 348; (h) 362; (i) 389; (j) 407; and (k) 423 K. (C) IR spectra of PdA sample in a flow of (a) 0.5% of $O_2$ in nitrogen at 298 K, then 1% CO, 0.5% $O_2$, $N_2$ balance at (b) 323; (c) 373; (d) 423; (e) 443; (f) 453; (g) 463; and (h) 473 K.

**TABLE 2**

**Assignment of Superoxide Species Detected by EPR on Ce Containing Catalysts**

| Signal | EPR parameters | Assignment |
|---|---|---|
| O1 | $g_\perp = 2.026$; $g_\parallel = 2.012$ | $Ce^{4+}$–$O_2^-$ at 2D-Ce edges |
| O2 | $g_z = 2.027$; $g_x = 2.018$; $g_y = 2.011$ | $Ce^{4+}$–$O_2^-$ at 2D-Ce surfaces |
| O3 | $g_z = 2.030$-29; $g_x = 2.016$-7; $g_y = 2.011$ | $Ce^{4+}$–$O_2^-$ at Pd–Ce interfaces |
| O4 | $g_\perp = 2.034$; $g_\parallel = 2.011$ | $Ce^{4+}$–$O_2^-$ at 3D-Ce entities |

$g = 2.005$ and with a splitting $A = 92$ G, which correspond to $Mn^{2+}$ impurities. This signal is observed in several EPR spectra presented in the study and is marked with asterisks (Figs. 5–8). Weak and narrow features with $g$ values close to $g_e$ (in the range $g = 2.01$ to 1.958) have been detected after 373 K CO-treatment, showing increasing intensity with cerium content in the samples. These probably correspond to the presence of small amounts of cerium-stabilized nitrosyl radicals resulting from the reduction of nitrates originating from incomplete decomposition of the palladium or, more probably, the cerium precursor.

Oxygen adsorption on CO-reduced cerium-containing samples yields superoxide radicals which correspond to different $Ce^{4+}$–$O_2^-$ species (Table 2). O1, O2, and O4 correspond to signals previously assigned (12, 13, 19), while O3 is here reported for the first time and is characteristic of Pd containing samples. All O-type signals reflect the formation, upon reduction with CO, of anion vacancies close to $Ce^{3+}$ ions which produce the superoxide species after oxygen adsorption. Comparison of the total amount of these species (as measured by double integration of spectra) produced in the absence and presence of Pd reveals a relatively strong promotional effect of palladium on radical formation (Fig. 5). For PdC, the amount of superoxide species formed following adsorption of 70 $\mu$mol $\cdot$ g$^{-1}$ of oxygen at 77 K reaches a maximum after reduction at 473 K. No maximum in the overall amount of $Ce^{4+}$–$O_2^-$ species is observed in the case of Pd39CA and Pd10CA (see Fig. 5B for the last case) after a similar adsorption (of 70 $\mu$mol $\cdot$ g$^{-1}$ of oxygen at 77 K). In the case of ceria supported Pd reduced at $T \geq$ RT and the support alone reduced to $T \geq 573$ K, warming to 298 K leads to the disappearance of the radicals, while further doses of $O_2$ admitted at 77 K ultimately generate a larger amount of radicals than those initially detected. In the case of samples reduced at 573 K, a maximum amount of these radicals is formed for PdC when 280 $\mu$mol $\cdot$ g$^{-1}$ of $O_2$ are added, while for ceria alone, the maximum amount of radicals is produced after treatment with 140 $\mu$mol $\cdot$ g$^{-1}$ (Fig. 5A).

A comparison of the spectra obtained for 10CA and Pd10CA following $O_2$ adsorption at 77 K on 373 K reduced samples is shown in Fig. 6. Only a weak signal O1 is produced for 10CA, whereas Pd10CA presents a spectrum formed mainly by the overlapping of signal O1, showing higher intensity than in the absence of Pd, and signal O2 (Fig. 6A(b)). Satisfactory simulation of the experimental spectrum is achieved only after 10% of a new, broader signal is included, this signal contributing particularly to the low and high magnetic field tails of the spectrum. The broad nature of this signal as well as its low intensity do not permit a conclusive definition of its $g$ values, with O2- or O3-type assignments (see Table 2) being possible. Nevertheless, a somewhat better fit (Fig. 6A(c)) is reached using the O3 parameters. Warming to 298 K after the experiment produced a similar spectrum (Fig. 6A(b)), but without the broad contribution. The greater reducibility of sample PdC allows observation of signal O3 following oxygen adsorption at 77 K on PdC reduced in CO at RT (Fig. 7a). The same signal but with greater intensity is detected after reduction in CO at 373 K. Note that the superoxide species are absent on the clean ceria support at reduction temperatures below 473 K (Fig. 5). Signal O3 disappears when the sample giving the spectrum of Fig. 7a is warmed to RT. In order to assess whether its absence is related to oxygen migration rather than vacancy reoxidation, subsequent doses

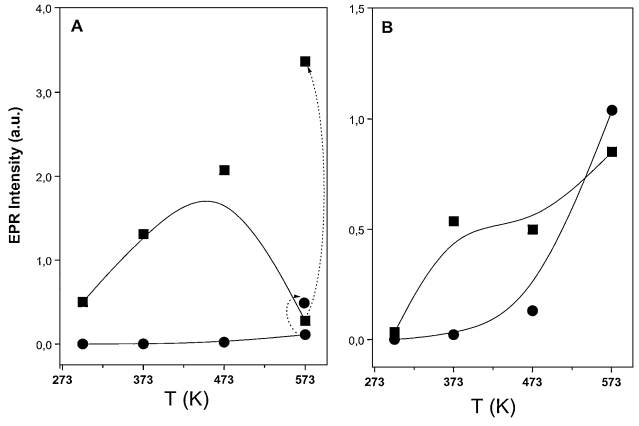


**FIG. 5.** Overall amount (measured by integration of EPR signals) of $Ce^{4+}$–$O_2^-$ radicals obtained upon adsorption of 70 $\mu$mol $\cdot$ g$^{-1}$ of $O_2$ at 77 K on samples reduced in CO at several temperatures ($T_r$). Circles, Pd-free; squares, Pd-containing samples. (A) C and PdC; (B) 10CA and Pd10CA specimens. For PdC and C at $T_r = 573$ K, the maximum amount of radicals after consecutive $O_2$ doses is presented by points marked with arrows. See text for details.

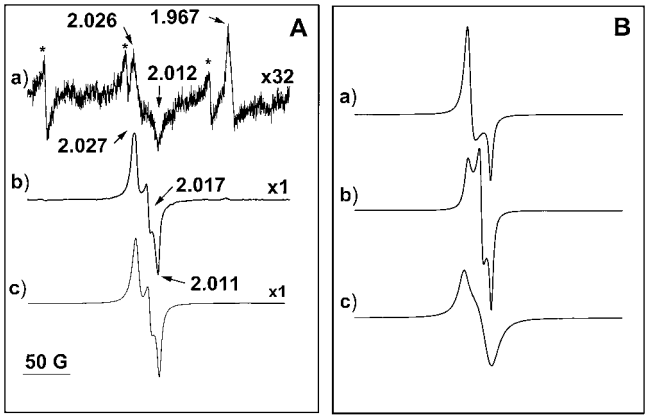


**FIG. 6.** (A) EPR spectra following $O_2$ adsorption at 77 K on samples reduced in CO at 373 K: (a) 10CA; (b) Pd10CA; (c) computer simulation of 6A(b) spectrum. (B) Individual components used in the computer simulation shown in 6A(c): (a) signal O1; (b) signal O2; (c) signal O3. See text for details of signal assignments.

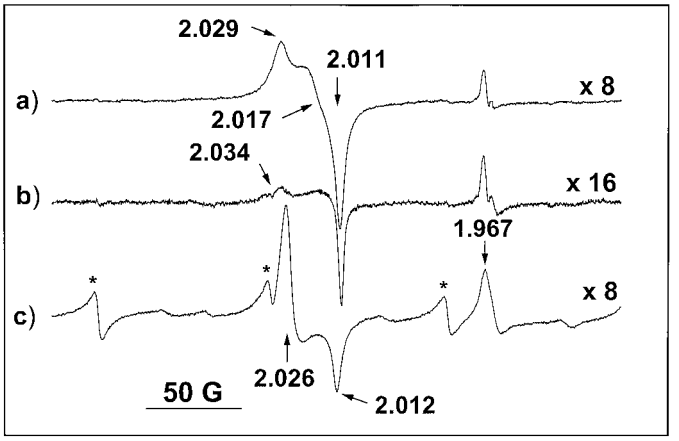


**FIG. 8.** EPR spectra following $O_2$ adsorption on samples treated in stoichiometric CO + $O_2$. (a) PdC at 323 K, adsorption at 77 K; (b) subsequent warming to RT; (c) Pd10CA, adsorption at 77K after treatment at 423 K.

of $O_2$ at 77 K (followed by outgassing) were performed. Results show a significant intensity decrease of signal O3, which finally disappears when about 280 $\mu$mol of $O_2$ per gram of sample have been admitted in the cell. Similarly, for Pd39CA, signal O3 is produced by $O_2$ adsorption at 77 K after CO reduction at RT (Fig. 7b), disappearing after subsequent warming to RT.

As indicated above, signals O1 and O2 have been observed in previous studies of dispersed ceria samples and attributed to $Ce^{4+}$–$O_2^-$ species formed, respectively, at edge and surface sites of 2-dimensional Ce entities (12, 13, 19). The definition of 2D-Ce particles is made on the basis of the existence of a direct chemical influence of alumina on the ceria surface properties, which is in turn reflected in the characteristics of the oxygen radicals adsorbed at ceria cations and gives no indication as to the size of the ceria entities. Signal O3 shows parameters that are different from those previously observed for similar species present in pure or supported ceria samples. This, along with the considerable promoting effect of Pd on their formation, suggests that the corresponding $Ce^{4+}$–$O_2^-$ species are formed at palladium–ceria interface sites. Their presence in the PdC samples indicates that such interfacial sites are formed over 3-dimensional ceria patches.

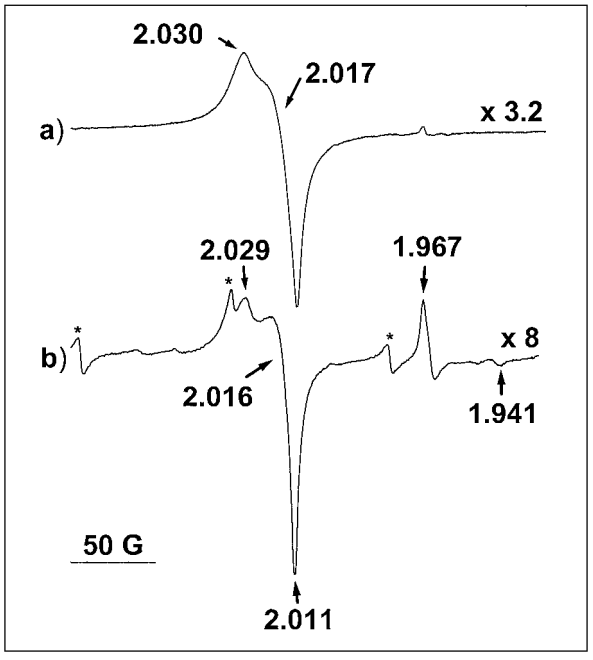


**FIG. 7.** EPR spectra following $O_2$ adsorption at 77 K on samples reduced in CO at RT; (a) PdC; (b) Pd39CA. See text for details of signal assignments.

The spectra obtained after oxygen adsorption on samples subjected to a stoichiometric CO + $O_2$ mixture also show the presence of superoxide radicals (Fig. 8). For PdC, a spectrum formed by the overlapping of signals O3 and O4 is observed after oxygen adsorption at 77 K on the sample pretreated in the stoichiometric gas mixture at 323 K (Fig. 8a). In contrast to reduction in pure CO, subsequent warming to RT does not lead to complete disappearance of the signals but rather to a decrease of ca. 60% of the original intensity (Fig. 8b). The intensity decrease results from a greater, almost complete loss of signal O3 than loss of signal O4. In the case of Pd10CA, only signal O1 is observed after adsorption on the sample subjected to CO + $O_2$ at 423 K (Fig. 8c).

## IV. DISCUSSION

### *Morphological Characteristics*

Electron microscopy data indicate that single microcrystal-like diffraction can be observed for PdC and the

ceria support. As the sample area covered by the electron beam undergoing diffraction is much larger than the size of the individual crystallites (as deduced from diffraction and TEM image data) and necessarily incorporates a number of these, this result indicates that groups of crystallites exist which have their lattices oriented in parallel. This probably arises from the topotactic decomposition of single cerium salt precursor crystals.

The effect is less marked for CA-supported samples, as is expected since the initial Ce nitrate crystals resulting from impregnation will in general be small and do not give rise on calcination to large collections of $CeO_2$ microcrystals sharing the same spatial orientation. However, some regions of the samples do show single crystal-like diffraction, indicating the original presence of some larger entities of the precursor salt. When this occurs, a [011] zone axis is always identified and the alumina diffraction rings also detected in the same TEM image contain spots, indicating preferential orientation of the $CeO_2$ crystallites with respect to the supporting carbon film mediated by a specific orientation of the underlying alumina. This implies an epitaxial relationship between the $CeO_2$ crystallite(s) and the alumina component, which may well give rise to an influence of alumina on the type of ceria crystal faces which are preferentially exposed in the calcined material. These faces appear also in the C specimen but less frequently.

Pd appears to be well dispersed for all supports, as there is little evidence of its presence in either EDS or electron diffraction data. Following the calcination treatment, Pd is expected to be fully oxidized in the starting materials. Although CO cannot be considered an inert probe and may lead to reduction to Pd(0) at 298 K of $PdO_x$ particles depending on their size (14, 15), significant disruption/aggregation of any zero-valent phase formed is not expected. This is supported by IR results (20) which show that once Pd is reduced, it appears insensitive to CO adsorption temperature in the range 140 K to RT so the adsorption process under conditions here is not likely to produce significant changes in dispersion. The IR spectra showing CO adsorption at 298 K (Fig. 3) suggest that the percentage of Pd in contact with ceria in the Pd*x*CA samples increases with increasing ceria content. A fraction of Pd in the Ce-rich zone of Pd39CA is in fact detected by EDS. The same CO adsorption experiment, using EPR after $O_2$ titration of the reduced surface centers, indicates that Pd promotes an extensive reduction of ceria and, consequently, a part of the active metal must be in direct contact with these reducible cerium oxide patches even for the Pd10CA sample.

*Formation of Sites for CO and $O_2$ Activation*

IR experiments performed under reaction conditions indicate that the presence of metallic $Pd^0$ sites is required to initiate the CO oxidation. This implies that CO must be electronically activated by the formation of a metal–CO covalent dative bond which transfers electron density into the molecular $2\pi^*$ orbitals, weakening the C–O bond (21). IR data also show that the presence of ceria drastically facilitates the formation of these CO activation sites. Contact with the stoichiometric $CO + O_2$ mixture leads, in this case, to Pd reduction at RT and generates the active phase required for catalytic reaction (Fig. 4). The large difference in Pd reducibility using ceria and alumina supports (ca. 100 K) cannot be attributed to a difference in Pd particle size since the failure to detect Pd by microscopy indicates a small average particle size for all samples, even after reaction. However, several studies have produced evidence for metal–ceria interactions which facilitate the mutual metal, Ce reduction/oxidation mechanism in response to changes in the gaseous atmosphere (12–14).

To discuss the activation of oxygen it is necessary to first consider the coverage of Pd particles with CO, reflected by the IR bands at 1980–1970 $cm^{-1}$ and 2099–2060 $cm^{-1}$ (Figs. 4A–4C). Using model $Pd/SiO_2$ systems, the CO surface coverage of the Pd metal phase during reaction remains approximately constant and close to unity while raising the temperature until the maximum conversion is reached (22). Just before reaching this temperature, desorption of CO occurs allowing greater quantities of oxygen to interact with the metal surface (22). This contrasts with the behavior of $Pt/Al_2O_3$, for example, where the surface coverage is progressively diminished while raising the temperature until a conversion of ca. 80% is reached. Between this temperature and the temperature required to attain 100% conversion, the CO coverage, as indicated by invariance in the stretching frequency, remained constant (23, 24). The PdA sample shows a significant shift in both carbonyl bands around temperatures equivalent to light-off indicating a loss of CO surface coverage by both desorption and reaction (Fig. 4C). For the mixed oxide supported samples, there is no appreciable change in CO coverage of the metallic Pd particles at temperatures where significant CO conversion is reached. The PdC catalyst shows similar behavior at low temperature but concurrent with the detection of $Pd^{2+}$ a drastic change in CO coverage is observed (Fig. 4A). Beyond this temperature the CO coverage remains constant (Fig. 4A (h–k)), consistent with the appearance of a plateau in $CO_2$ production (detected by IR) and CO conversion (reaction results).

This invariance in CO coverage implies that, at temperatures below which PdA does not oxidize CO ($T \leq 423$ K), ceria containing samples must provide an alternate pathway for oxygen activation that does not require the CO-free sites on the metal surface. If such a pathway exists, then in the presence of Pd this should produce a route to CO oxidation even at RT. Although there is general agreement that anionic vacancies at the ceria surface are the active sites for oxygen activation (8), controversy exists regarding the specific activated oxygen species that interacts with CO. While

several authors consider that superoxide $O_2^-$ species can attack CO molecules (24–26), others favor a more reduced species, typically (diamagnetic) oxide anions at the metal–support interface (13, 27). Previous EPR experiments show that superoxide radicals bonded to Ce ions do not react extensively with CO adsorbed on Pt at 423 K, reducing the likelihood of the former pathway as a route to $CO_2$ formation (13).

Regarding the anion vacancies on ceria, EPR data suggests significant involvement of O2 and O3 vacancy types in the generation of diamagnetic (more reduced than $O_2^-$) oxygen species under reaction conditions. This is inferred from a comparison of data obtained after CO and after CO + $O_2$ treatments, which show significant decreases of the superoxide signals for the latter treatment. On the other hand, the different thermal stability observed for the adsorbed superoxide species indicates that the vacancies giving rise to species O3, i.e., those assigned to the Pd/3D-Ce interface, undergo the faster reoxidation and can therefore be envisaged as being the most effective site for supply of activated oxygen. This is demonstrated by the exclusive (among O-type species) disappearance of this signal upon warming from 77 K to RT and the inability to recover its initial intensity upon subsequent $O_2$ dosing at 77 K. For Pd10CA, the anion vacancy producing signal O2 may also be a source of reactive oxygen. In this case, the 2-dimensional ceria particles are clearly involved. The thermal stability differences mentioned in connection with the creation, by CO, and oxidation, by $O_2$, of O-type ceria vacancies suggest that the Pd/3D-Ce contact is more efficient than the Pd/2D-Ce interface for oxygen activation for CO oxidation.

Considering the reactivity of oxygen vacancies, it can be concluded that the ca. 6 nm ceria patches of Pd10CA contain contributions from 2D-Ce-like structures, i.e., those having significant contact with alumina, while the 11 nm patches of Pd39CA act chemically like 3D-Ce structures. The geometrical influence of alumina leading to preferential orientation presented by ceria particles supported on this material is common to all Pd*x*CA samples.

### *CO + $O_2$ Reaction*

The behavior of PdA for CO oxidation is consistent with a Langmuir–Hinshelwood mechanism, as observed for model $Pd/SiO_2$ catalysts (22). At temperatures below those giving maximum conversion, the CO coverage of metallic Pd particles is close to unity and the rate-determining step is the creation of empty sites by desorption of CO where $O_2$ can be activated (22). In the case of preoxidized samples used here, the catalytic activity is very low until the temperature is reached where extensive reduction of Pd by CO can take place. The subsequently reduced surface is then in a state where activation of CO can occur at a coverage which, being less than unity, allows simultaneous activation/dissociation of oxygen.

The presence of ceria reduces the light-off temperature by ca.130 K (Fig. 1) due to both the ease with which metallic Pd is formed (Fig. 3), which facilitates the activation of CO, and the existence of Pd–Ce interactions where additional sites for oxygen activation are readily generated. These findings are analogous to those observed for other ceria-supported noble metals (13, 14), although the detection of such species even at RT seems to be a unique characteristic of Pd. The light-off curves show that PdC contains active sites that experience deactivation at temperatures $\geq$423 K. At this temperature, $Pd^{2+}$ species were detected by DRIFTS and these sites are thought to be less effective for CO activation (22, 27). Oxidation of Pd(0) to Pd(II), with a corresponding reduction of Ce(IV) to Ce(III), could explain the presence of $Pd^{2+}$ species if the sharp band at 2152 $cm^{-1}$ is due to reduced $Ce^{\delta+}$ ($\delta \leq 3$) sites. A contribution from $Ce^{3+}$-like species has been observed in other ceria containing samples in the same temperature range (14, 29, 30). However, this assignment to $Ce^{3+}$ is unlikely, as the 2152 $cm^{-1}$ band was not detected for the ceria support alone during CO reduction up to 523 K. On the other hand, the coexistence of both oxidic and metallic Pd as detected by IR indicates that this oxidation process is limited to the metal–support interface. As the rise in CO conversion with temperature above 473 K for the PdC catalyst is due to reaction on the ceria support, the alternative possibility that only a fraction of the active Pd particles are extensively oxidized can be eliminated, yielding the conclusion that the contribution of Pd to the catalytic activity at medium-high temperatures is removed. The absence of any permanent loss of activity after the first reaction run of PdC eliminates interpretations such as encapsulation of the metal (as observed for reduced Pd/Ceria samples) (20) and/or the formation of stable local Pd–Ce mixed oxide structures as possible chemical reasons for the observed reaction behavior. The data suggest, therefore, that at high temperature, Pd is maintained in a partly oxidized state which seriously affects its activity and is only reduced again at low temperature by the reaction mixture. One possible explanation could be that, at higher temperatures, the surface of ceria in PdC suffers a Pd-induced transformation to a reduced (more reduced than in Pd*x*CA) state with higher basicity in the $O^{2-}$ ions, which in turn stabilizes Pd as $Pd^{2+}$ at the interface and hinders the CO + $O_2$ reaction. Cooling toward RT restores the inital situation by partial reoxidation of the ceria surface. This complex behavior is also expected for subsequent reactions, although the CO conversion plateau exhibited here (Fig. 1) is much less pronounced.

The most interesting catalytic result obtained here is connected with the mixed oxide supports. In contrast to the ceria supported Pd species, the Pd10CA, Pd39CA samples

present less complex behavior and in particular show only minimal sensitivity to the Pd particle size (over the range studied) or the ceria reducibility (Fig. 1). Size/structure insensitivity has been already reported for $Pd/SiO_2$ systems (21). The mixed oxide support shows CO conversion which increases moderately with ceria loading, suggesting that more facile production/oxidation of ceria anionic positions located in the interface between 3D-Ce particles (i.e., particles less affected by direct chemical contact with alumina) and Pd is the origin of the observed phenomenon. The marked differences with the PdC sample can be ascribed to modification of the Pd–Ce interaction originating in the different faces exposed by ceria in the mixed CA supports and the ceria which finally leads to different chemical phenomena at medium-high reaction temperatures. The greater degree of ceria reduction attained by PdC compared with Pd39CA above 373 K, as deduced from EPR experiments, is likely to be the origin of this effect. As the activation–dissociation of oxygen consists of the transfer of electrons from ceria to the molecule, a more reduced ceria surface would present a greater ability to activate oxygen. However, above a certain temperature, it is apparent that this readily activated oxygen is able to oxidize Pd at the metal–support interface. Alumina, therefore, is able to stabilize specific (geometric) ceria local structures which adequately promotes the activity of palladium.

This promoting effect is akin to observations using $Cu/CeO_2$ where the Cu/3D-Ce interaction enhances reactivity when compared with Cu/2D-Ce (11, 12), but is in contrast to the behavior of $Pt/CeO_2$ where metal particles in contact with 2D-Ce patches would appear to be the most active (13). This correlates with the increasing work function from Cu to Pt (31), suggesting that ceria vacancies in 2D-Ce patches are more readily formed but have lower reactivity, i.e., undergo reoxidation with greater difficulty, hindering subsequent formation of active oxygen species. Evidence for greater resistance to reoxidation of these 2D-Ce particles has been reported (19).

## V. CONCLUSIONS

The oxidation of CO has been studied for four Pd catalysts supported on alumina, ceria, and ceria/alumina. When ceria is present, the onset of reaction between CO and $O_2$ occurs at temperatures ca. 130 K below that shown by the alumina supported catalyst. Ceria facilitates CO activation by formation of metallic $Pd^0$ at temperatures around 298 K and $O_2$ activation by generation of vacancies at the Pd–Ce interface, which are created and readily oxidized from 298 K. In contrast with other noble metals, Pd is unique in activating CO and $O_2$ at such low temperatures. These reduction/oxidation processes may be enhanced by a Pd–Ce electronic interaction. The results of catalytic tests and characterizations indicate that the promoting effect in CO conversion reaches its maximum when metallic Pd is in contact with 3-dimensional ceria particles exhibiting specific orientations. These are a direct consequence of the underlying alumina support. For Pd/ceria, a plateau in the CO conversion below 100% is observed and attributed to the formation of less active/inactive $Pd^{2+}$ species. This effect is not apparent for ceria/alumina samples. Oxidation of palladium is thought to occur specifically at the Pd–Ce interface which leads to subsequent blocking of reactant mobility across it. The maximum in ceria promotion as a function of the catalyst cerium content is a balance, driven by ceria, between the ability to activate–dissociate oxygen and maintain Pd in a metallic state at the metal–support interface.

## ACKNOWLEDGMENTS

We thank the Ministerio de Educación of Spain for a postdoctoral contract (to M.F.-G.) and the Comunidad de Madrid for a postdoctoral grant and for support under the "Ayudas para Estancias Breves en el Extranjero" program (to A.M.-A.). We also thank the Royal Society (London) for a European Exchange Fellowship (M.F.-G.) and a University Research Fellowship (J.A.A.). Mr. F. Sánchez Constela is thanked for recording the EPR spectra. Support from CAICYT (Project MAT 97-0696-CO2-O1) and CAM (Project 06M/085/96) is fully appreciated.

## REFERENCES

1. Yao, H. C., and Yu-Yao, Y. F., *J. Catal.* **84**, 254 (1986).
2. Engler, B., Koberstein, E., and Schubert, P., *Appl. Catal.* **48**, 71 (1989).
3. Miki, T., Hareda, M., Kakuta, N., Ueno, A., Tateishi, S., Matsura, S., and Sato, M., *J. Phys. Chem.* **94**, 6464 (1990).
4. Ozawa, M., and Kimura, M., *Mater. Sci. Lett.* **9**, 291 (1990).
5. Dictor, R., and Roberts S., *J. Phys. Chem.* **93**, 5846 (1989).
6. Su, E. C., and Rothshild, W. G., *J. Catal.* **99**, 506 (1989).
7. Hardacre, C., Ormerod, R. M., and Lambert, R. M., *J. Phys. Chem.* **98**, 10901 (1994).
8. Trovarelli, A., *Catal. Rev. Sci. Eng.* **38**, 439 (1996).
9. Searles, R. A., *Stud. Surf. Sci. Catal.* **116**, 23 (1998).
10. Fernández-García, M., Gómez-Rebollo, E., Guerrero-Ruiz, A., Conesa, J. C., and Soria, J., *J. Catal.* **172**, 146 (1997).
11. Martínez-Arias, A., Soria, J., Cataluña, R., Conesa, J. C., and Cortés-Corberán, V., *Stud. Surf. Catal.* **116**, 591 (1998).
12. Martínez-Arias, A., Fernández-García, M., Soria, J., and Conesa, J. C., *J. Catal.* **182**, 367 (1999).
13. Martínez-Arias, A., Coronado, J. M., Cataluña, R., Conesa, J. C., and Soria, J., *J. Phys. Chem. B* **102**, 4357 (1998).
14. Bensalem, A., Muller, J. C., Tessier, D., and Buzon-Verduraz, F., *J. Chem. Soc. Faraday Trans.* **92**, 3233 (1996).
15. Hollins, P., *Surf. Sci. Rep.* **16**, 51 (1992).
16. Fernández-García, M., Anderson, J. A., and Haller, G. L., *J. Phys. Chem.* **100**, 16247 (1996).
17. Tarasov, A. L., Shets, V. A., and Kazankii, V. B., *Kin. Catal.* **30**, 396 (1989).
18. Lee, C. W., Yu, J.-S., and Kevan, L., *J. Phys. Chem.* **96**, 7747 (1992).
19. Martínez-Arias, A., Coronado, J. M., Conesa, J. C., and Soria, J., *in* "Rare Earths" (R. Sáez-Puche and P. Caro, Eds.), Complutense, Madrid, 1997.
20. Badri, A., Binet, C., and Lavalley, J. C., *J. Chem. Soc. Faraday Trans.* **92**, 1603 (1996).
21. Pacchioni, G., and Bagus, P. S., *J. Chem. Phys.* **93**, 1209 (1990).

22. Xu, X., and Goodman, D. W., *J. Phys. Chem*. **97**, 7711 (1993).
23. Anderson, J. A., *J. Chem. Soc. Faraday Trans.* **88**, 1197 (1992).
24. Anderson, J. A., *Catal. Lett.* **13**, 363 (1992).
25. Zhang, X., and Klabunde, K. J., *Inorg. Chem*. **31**, 1706 (1992).
26. Li, C., Domen, K., Moruya, K., and Onishi, T., *J. Am. Chem. Soc.* **111**, 7683 (1989).
27. Tarasov, A. L., Przheval'skaya, L. K., Shevts, V. A., and Kazanskii, V. B., *Kinet. Catal.* **29**, 1020 (1989).
28. Jin, T., Okuhara, T., Mains, G. J., and White, J. M., *J. Phys. Chem*. **91**, 3310 (1987).
29. Di Monte, R., Fornasiero, P., Kaspar, J., Gibitosa, G., and Graziani, M., *Stud. Surf. Sci. Catal.* **116**, 559 (1998).
30. Morterra, C., Bolis, V., and Magnacca, G., *J. Chem. Soc. Faraday Trans.* **92**, 1991 (1996).
31. "CRC Handbook of Chemistry and Physics," 72nd ed., CRC Press, Boca Raton,1992.